A Thermodynamic and Structural Study of Myelin Basic Protein in Lipid Membrane Models

P. Rispoli,* R. Carzino,* T. Svaldo-Lanero,* A. Relini,* O. Cavalleri,* A. Fasano,† G. M. Liuzzi,† G. Carlone,‡ P. Riccio,‡ A. Gliozzi,* and R. Rolandi*

*Department of Physics, University of Genoa, 16146 Genova, Italy; †Department of Biochemistry and Molecular Biology, University of Bari, 70126 Bari, Italy; and ‡Dipartimento di Biologia, Difesa e Biotecnologie Agro-Forestali, University of Basilicata, 85100 Potenza, Italy

ABSTRACT Myelin basic protein (MBP) is a major protein of the myelin membrane in the central nervous system. It is believed to play a relevant role in the structure and function of the myelin sheath and is a candidate autoantigen in demyelinating processes such as multiple sclerosis. MBP has many features typical of soluble proteins but is capable of strongly interacting with lipids, probably via a conformation change. Its structure in the lipid membrane as well as the details of its interaction with the lipid membrane are still to be resolved. In this article we study the interaction of MBP with Langmuir films of anionic and neutral phospholipids, used as experimental models of the lipid membrane. By analyzing the equilibrium surface pressure/area isotherms of these films, we measured the protein partition coefficient between the aqueous solution and the lipid membrane, the mixing ratio between protein and lipid, and the area of the protein molecules inserted in the lipid film. The penetration depth of MBP in the lipid monolayer was evaluated by x-ray reflectivity measurements. The mixing ratio and the MBP molecular area decrease as the surface pressure increases, and at high surface pressure the protein is preferentially located at the lipid/water interface for both anionic and neutral lipids. The morphology of MBP adsorbed on lipid films was studied by atomic force microscopy. MBP forms bean-like structures and induces a lateral compaction of the lipid surface. Scattered MBP particles have also been observed. These particles, which are 2.35-nm high, 4.7-nm wide, and 13.3-nm long, could be formed by protein-lipid complexes. On the basis of their size, they could also be either single MBP molecules or pairs of c-shaped interpenetrating molecules.

INTRODUCTION

The myelin sheath is a multilamellar membrane tightly wrapped around the axon segments in the central and peripheral nervous systems. Being an insulator, it confines the electrical activity to the unmyelinated regions called nodes of Ranvier, with a consequent increase in the conduction velocity of the action potential. In the central nervous system (CNS) the myelin sheath is formed by flattened extensions of cells (oligodendrocytes) that wrap around the axon to form a cylindrical scroll a few tens of micrometers in diameter. As the oligodendrocyte wraps around the axon, all the spaces between its plasma membrane, both cytosolic and exoplasmic, are reduced, resulting in a close apposition of both the cytosolic faces and exoplasmic faces of the plasma membrane. A myelin sheath section, perpendicular to the axon axis, shows regularly alternating rings of exoplasm, plasma membrane, and cytoplasm. The aqueous layers are 3–4-nm thick (1–4).

Proteins constitute 30% of the myelin dry weight in the CNS. The major ones are proteolipid protein (PLP, 50% of total protein content) and myelin basic protein (MBP, 20% of total protein). PLP is an archetypal intrinsic membrane protein with several segments that span the membrane and are connected by loops exposed to the intracellular and extracellular aqueous environments. In contrast, MBP has the overall amino acid polarity typical of the water-soluble proteins, and it is located on the cytosolic surface of the oligodendrocyte membrane. Much experimental evidence indicates that both these proteins are particularly important for the structural integrity of the myelin sheath. The close apposition of the cytosolic faces of the plasma membrane may result from MBP-MBP and MBP-PLP interactions, whereas apposition of the exoplasmic faces may result from PLP-PLP interactions (4).

The integrity of the myelin sheath is fundamental for the fast saltatory conduction of the signal along the axon. Stacking abnormalities, such as the occurrence of myelin with an unusually large periodicity, have been reported for a variety of human and animal diseases (5). Therefore, it is of the utmost importance to understand the nature of the interactions that maintain the structural integrity of the myelin sheath. In particular, we focused our attention on the interaction of MBP with membrane lipids. The physical bases of this interaction are clear, but many details are not yet understood. MBP contains 10 histidines, 13 lysines, and 18 arginines; at neutral pH it has a net positive charge of ~20 elementary charges, resulting from the balance between negatively charged and positively charged residues. Its isoelectric point is above 10. Due to its overall positive charge, MBP interacts electrostatically with the polar heads of anionic lipids (6,7). However, it also contains segments composed of 5–10 hydrophobic and neutral amino acids and associates hydrophobically with lipids and detergents (7–9).

Submitted December 29, 2006, and accepted for publication May 2, 2007.

R. Carzino and P. Rispoli contributed equally to this work.

Address reprint requests to Ranieri Rolandi, E-mail: rolandi@unige.it.

R. Carzino is on leave to IIT Foundation, via Morego 3, 16163 Genova, Italy.

Editor: Thomas J. McIntosh.

0006-3495/07/09/1999/12 $2.00

doi: 10.1529/biophysj.106.103820

Water-soluble MBP belongs to the class of intrinsically unstructured proteins (IUP). In water it has a random coil conformation and acquires some coherent secondary structure when it is added to a lipid environment (7). MBP, extracted in a lipid-bound form (10), shows a defined secondary structure (11,12). Until now, all attempts to determine the MBP structure in intact myelin have failed. Therefore, structural studies have often been performed by using plasma membrane models such as vesicles and Langmuir and Langmuir-Blodgett (LB) films. Beniac et al. (13), by using transmission electron microscopy images and computer simulation, showed that the MBP molecules attached to a lipid monolayer assume a planar distribution and a toroidal shape of ~11 nm in diameter. Bates et al. (14) and Ishiyama et al. (15) observed that a recombinant hexahistidine-tagged 18.5-kDa isoform of murine MBP forms planar arrays of lamellae with a 4.8-nm repeat in monolayers of an equimolar mixture of phosphatidylinositol and nickel-chelating lipid.

Particles of 3–4-nm diameter appear on the periphery of the lamellae and seem to be coalescing into fibrous structures. Atomic force images of MBP adsorbed on LB films show the presence of bean-shaped granules that could be single molecules (16). Evidences about the penetration of MBP molecules into the lipid leaflet come from x-ray, neutron reflectivity, and electron paramagnetic resonance measurements on liposomes and Langmuir and LB films. Murthy et al., from x-ray scattering measurements concluded that MBP increases the repeat period of phosphatidylglycerol multilayers and that the basic protein penetrates into the bilayer (17). MacNaughtan et al., by using x-ray diffraction measurements, found that MBP does not change the lipid bilayer thickness of LB films of cerebroside sulfate and cholesterol but changes the electronic density profile of the lipid/water interface region. These authors estimated that the size of MBP perpendicular to the membrane surface is ~3 nm (18). Haas et al., from x-ray and neutron reflectivity measurements on LB films of dimyristoyl-Lα-phosphatidic acid (DMPA) and MBP, concluded that MBP forms a 1-nm-thick layer between the phospholipid polar heads (19). Cristofolini et al., using x-ray reflectivity measurements, found that MBP destroys the structural regularity of dipalmitoylphosphatidylglycerol (DPPG) monolayers at the air water/interface (20). Bates et al. studied the interaction of recombinant murine MBP isomers with large unilamellar vesicles of physiological composition by electron paramagnetic resonance and showed that the N-terminal and C-terminal sites in the normal MBP are located below the plane of the phospholipid headgroups, whereas in the less cationic form that predominates in multiple sclerosis the C-terminal domain dissociates from the membrane (9). In addition, they found that segments 83–92 (corresponding to the human segments 86–95) in the normal MBP is an amphipathic α-helix, penetrating up to 12 Å into the bilayer (21); in the less cationic form this segment forms a shorter helix that is highly surface exposed and thus more susceptible to proteases (22).

In this article we investigated the physical interaction of MBP with phospholipid membranes by using different techniques. Since we were interested in defining the role of physical parameters as lipid charge and surface pressure, we used as simple an experimental model as possible. As membrane models, we have used Langmuir and LB films of anionic and neutral phospholipids. By using a method proposed by Schwarz (23,24), we measured the partition coefficient of MBP between water and the lipid membrane as well as the area that MBP occupies in the lipid film as a function of the surface pressure. From x-ray reflectivity measurements we obtained the electron density profile of MBP from which the degree of penetration and the thickness of the protein layer at the lipid/water interface were evaluated. The in-plane morphology of the protein layer was studied by atomic force microscopy (AFM).

MATERIALS AND METHODS

Materials

MBP was extracted from bovine brain and spinal cord and purified in the water-soluble, lipid-free form according to the method of Deibler et al. (25). The protein content was determined using the Bio-Rad Bradford reagent (Bio-Rad Laboratories, Hercules, CA) and a microassay procedure. Protein concentration was determined spectrophotometrically using an $\varepsilon = 10{,}300$ $M^{-1}cm^{-1}$ at 276 nm (26).

1,2-Dipalmitoyl-*sn*-glycero-3-phospho-L-serine (DPPS) (purity >99%) was purchased from Sigma Aldrich (Milan, Italy). DMPA, 1,2-dimyristoyl-*sn*-glycero-3-phosphocholine (DMPC), and 1,2-dipalmitoyl-*sn*-glycero-3-phosphocholine (DPPC) (purity >99%) were purchased from Avanti Polar Lipids (Alabaster, AL). DPPS was dissolved in chloroform (≥99.5%, Fluka, Milwaukee, WI), whereas DMPA, DPPC, and DMPC were dissolved in chloroform-methanol (Aristar grade, BDH, Milan, Italy) 3:1 (v/v). Lipid concentrations were in the range between 0.2 and 0.4 mg/ml.

Surface pressure-area isotherms

Monolayers were formed by spreading an aliquot of lipid solution (typically 60–80 μl) on 10 mM Tris(hydroxymethyl)aminomethane, titrated to pH 7.4 with HCl. Milli-Q (Millipore, Bedford, MA) filtered water with resistivity >18 MΩ/cm was used. Surface pressure-area isotherms were measured in a type 622D1 LB trough from Nima Technology (Coventry, UK) at a barrier compression speed of 5 cm^2/min. The compression rate was chosen to obtain equilibrium isotherms. Equilibrium surface pressure values were checked measuring the surface pressure at fixed areas for different amounts of lipid and protein. To prepare protein-lipid films, the lipid solutions were spread on a subphase containing the appropriate amount of MBP. All the experiments were performed at room temperature.

Thermodynamics of the MBP/phospholipid membrane interaction

Our experimental system is a phospholipid Langmuir film spread on an aqueous subphase containing MBP. On the basis of previous findings, the phospholipid is treated as an insoluble surfactant that can be located only at the air/subphase interface. Therefore, its concentration in the bulk subphase is negligible. MBP, on the other hand, is considered a soluble surfactant that may partition between the interface and the bulk. Therefore, MBP molecules can mix with lipid molecules at the air/subphase interface, and MBP bulk

concentration is not negligible. The measurable quantities are the total amounts of lipid and protein, the surface area, and the surface pressure of the film while the temperature is kept constant. The aim of this analysis is to determine the partitioning of MBP between the lipid monolayer and the aqueous subphase. This parameter will allow us to calculate the film area occupied by protein molecules. Following Schwarz and Taylor (24), the law of mass conservation for this system can be written in the following form:

$$n_p^o = n_l r + n_p^s \quad \text{with} \quad r = \frac{n_p}{n_l}, \tag{1}$$

where n_p^o is the total amount of the added protein, n_l is the total amount of lipid, r is the mixing coefficient, n_p^s is the amount of protein in the aqueous subphase, and n_p is the amount of protein in the interfacial domain. These amounts are conveniently expressed as number of moles.

According to Schwarz and Taylor (24), when the protein concentration in the subphase is small enough to neglect nonideal interactions and the change of the chemical potential of water for protein addition is negligible, r and n_p^s are solely determined by the surface pressure π and the lipid area per mole, A^*, which is the ratio between the film area A and n_l. Therefore, keeping the surface pressure and the lipid area per mole fixed, r and n_p^s also remain constant and the mass conservation law is a linear function of n_p^o and n_l. Since these quantities are experimentally available, the plot of the former as a function of the latter provides the values of r and n_p^s.

To obtain the film area occupied by MBP molecules, we must consider that protein adsorption increases the surface area of the film. The area increase per lipid mole, ΔA^*, can be measured, as a function of the surface pressure, by comparing the surface pressure/area equilibrium isotherms in the presence and in the absence of protein.

This area increase results both from the surface area occupied by adsorbed protein molecules, rA_p, and from the variation of the area occupied by each lipid molecule as a consequence of lipid-protein interaction, ΔA_l.

$$\Delta A^* = \Delta A_l + rA_p. \tag{2}$$

Considering that the lipid packing density may change in the vicinity of inserted protein molecules and that this solvation effect should increase in proportion to r, ΔA_l would be included in the apparent value of A_P. Therefore, we have calculated the protein molecular area as a function of the surface pressure according to the equation

$$A_p(\pi) = \frac{\Delta A^*(\pi)}{r}. \tag{3}$$

X-ray reflectivity measurements

X-ray reflectivity measurements were performed with a butterfly-type x-ray reflectometer assembled at the Dept. of Physics of Genoa University. The apparatus is described in detail in D'Acapito et al. (27). The design and mechanical parts were provided by JJ-X-ray, Danish Science Design (Liseleje, Denmark). The x-ray source is a conventional glass tube (PW 2273/20, Long Fine Focus, Cu anode, PW 1316 tube shield, Philips Analytical (Eindhoven, The Netherlands) fed by a PW 1830/40 high power generator (Philips Analytical). The reflectometer is equipped with a Langmuir trough specifically designed and built for x-ray measurements by R&K (Potsdam, Germany).

The intensity of the beam reflected by the Langmuir film is measured by an energy-dispersive Si detector (Amptek, Bedford, MA) as a function of the incidence angle. The detector is connected to a multichannel analyzer (MULTIPORT-16E/R, Oxford Instruments Nuclear Measurements Group, Oak Ridge, TN) whose output is read via an Event Control Block electronic interface (Risø National Laboratory, Roskilde, Denmark, and JJ X-Ray). Monolayers were formed by spreading 200 μl of a 0.4 mg/ml lipid solution on the same subphase used for surface pressure-area isotherms. For measurements in the presence of MBP, the monolayer was spread immediately after filling the trough with the protein solution. The protein concentration was 1.1×10^{-8} M in the experiments at low surface pressure and 2.2×10^{-8} M in the experiments at intermediate and high surface pressure. After solvent evaporation, the monolayer was compressed to the desired surface pressure. The surface pressure increase due to protein adsorption was recorded until it reached the saturation value. At this point x-ray reflectivity measurements were performed. The experimental data were analyzed with PARRAT32 software (Christian Braun, HMI, Berlin, Germany).

Atomic force microscopy

The samples for AFM were prepared by the LB technique using the dipper of the Nima Langmuir trough (type 622D1, Coventry, UK). Monomolecular films spread on a suitable aqueous subphase were transferred by vertical dipping on hydrophilic glass disks (12 mm in diameter) at a surface pressure of 30 mN/m. The dipping rate was 2 mm/min. The deposition procedure started with the glass disk immersed in the subphase. The layers exposing hydrophobic tails were deposited during upstrokes (odd layers), whereas the layers exposing hydrophilic groups were deposited during downstrokes (even layers). After every odd layer deposition, the sample was allowed to dry in air for a few minutes. The deposition ratio, which is the ratio between the reduction of the film area and the area of the glass disk immersed/emersed for each stroke, was near 1 for odd layers and ~0.7 for even layers. Since DPPS and DPPC do not form multilayers easily, five layers were deposited from a DMPA film formed on 10^{-4} M $ZnCl_2$, with the aim of obtaining a homogeneous and relatively defect-free lipid film to support the final protein-lipid layer.

On this film a protein-lipid layer (either DPPS/MBP or DPPC/MBP) was deposited by a downstroke from a protein-lipid film formed on 10 mM Tris, pH 7.4. After this last downstroke, the sample was allowed to drop into a container immersed in the subphase; then it was transferred from the container to the AFM sample holder, carefully keeping a solution film on its upper surface. The dried lower surface of the glass disk was attached to a Teflon-covered steel disk by using an adhesive tape and mounted on the AFM sample holder. Tapping mode AFM images were obtained in a liquid environment (10 mM Tris, pH 7.4) at room temperature using a Multimode scanning probe microscope (Digital Instrument, Santa Barbara, CA) equipped with an E scanning head (maximum scan size 10 μm) and controlled by a Nanoscope IV controller. V-shaped gold-coated Si_3N_4 cantilevers (type DNP; Veeco, Santa Barbara, CA; 200-μm length) with nominal spring constant of 0.06 N/m and tip radius 20–60 nm were used. The drive frequency was in the 4–7 kHz range, and the scan rate was in the 0.5–1 Hz range. The roughness analysis was performed using the Nanoscope software (Nanoscope 5.12 b49). The roughness is the root mean square of the image height measured with respect to an arbitrary level.

RESULTS

Thermodynamic study of the DMPC-MBP and DPPS-MBP complex

Fig. 1 shows equilibrium surface pressure/area isotherms of DMPC (*a*) and DPPS (*b*) Langmuir films spread on subphases containing different amounts of MBP. In both cases MBP expands the isotherms, especially at low surface pressures. At high surface pressures (>25 mN/m) the expansion effect is almost independent of the MBP concentration. High concentrations of MBP seem to induce the shrinking of the films (curves *4* of Fig. 1, *a* and *b*) at high surface pressures. Notably, MBP shifts the liquid-expanded-liquid-condensed phase transition of the DPPS film to higher surface pressures. The effects induced by MBP on DMPC and DPPS monolayers,

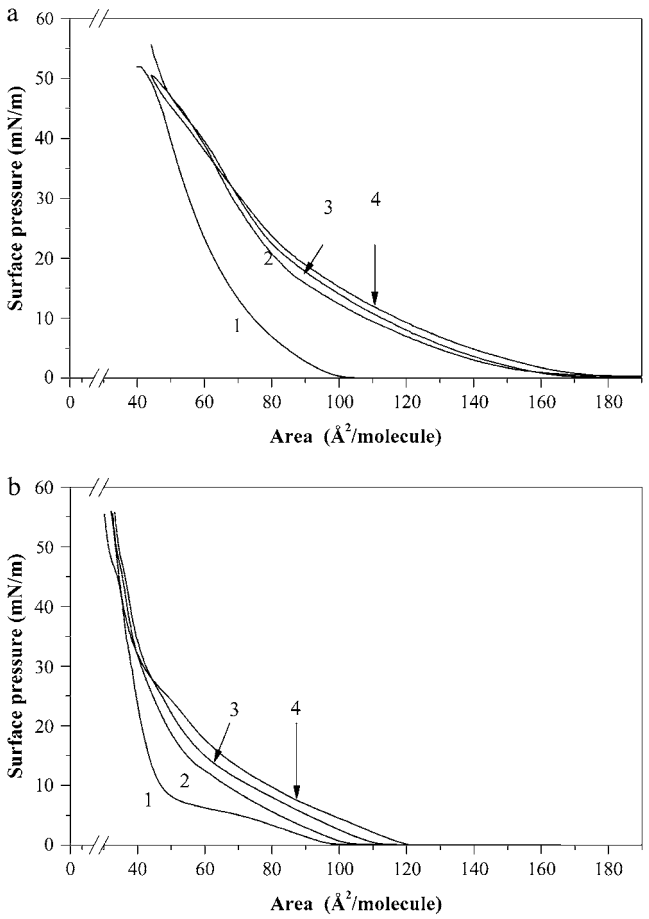

FIGURE 1 Surface pressure-surface area isotherms of DMPC and DPPS Langmuir films with different amounts of MBP in the water subphase buffered at pH 7.4. (*a*) DMPC films, MBP amount: (*1*) no MBP; (*2*) 0.36 nM; (*3*) 0.41 nM; and (*4*) 0.48 nM. (*b*) DPPS films, MBP amount: (*1*) no MBP; (*2*) 0.9 nM; (*3*) 1.3 nM; and (*4*) 2.1 nM.

such as isotherms expansion, shrinking of the film areas at surface pressures higher than 35 mN/m, and shift of the liquid-expanded-liquid-condensed phase transitions to higher surface pressures, are similar to those found with other phospholipid films such as DPPC, DMPA, DPPA, and DLPA (16,19; N. Lanteri, H. Haas, and A. Gliozzi, unpublished results).

According to the thermodynamic analysis of protein/lipid monolayer interaction (vide supra), the mass conservation law expressed by Eq. 1 can be used to measure the number of protein molecules in the bulk, n_p^s, and the mixing ratio r, which in turn yields the number of protein molecules at the air/water interface. The thermodynamic model reported above does not take into account the phase transition occurring in DPPS monolayers and the shift of the phase transition to higher surface pressures induced by the presence of MBP. Therefore, in the case of DPPS/MBP monolayers we have applied this analysis only to a few surface pressure values for which we have considered the effect of the phase transition negligible. For DMPC/MBP films the analysis was applied advantageously up to a surface pressure of 20 mN/m. At higher values the area increase induced by the protein is too small and comparable with the experimental errors.

To obtain the values of n_p^o and n_l at fixed surface area and surface pressure, we followed the approach of Schwarz and Taylor (24). Several series of isotherms at different protein amounts were measured; each series corresponded to a different fixed amount of lipid. All the isotherms were similar to the one shown in Fig. 1. From these curves, the area increase per mole of lipid, ΔA^*, at fixed surface pressure values was determined as a function of the total amount of protein, n_p^o, and lipid, n_l. The plot of ΔA^* versus n_p^o (Fig. 2 *a*) shows that the dependence of the area increase on the MBP total concentration is nicely described by straight lines whose slope depends on the amount of lipid forming the monolayer. At a fixed ΔA^*, each of these lines provides a pair of n_l and n_p^o values required for plotting the conservation mass equation (Fig. 2 *b*).

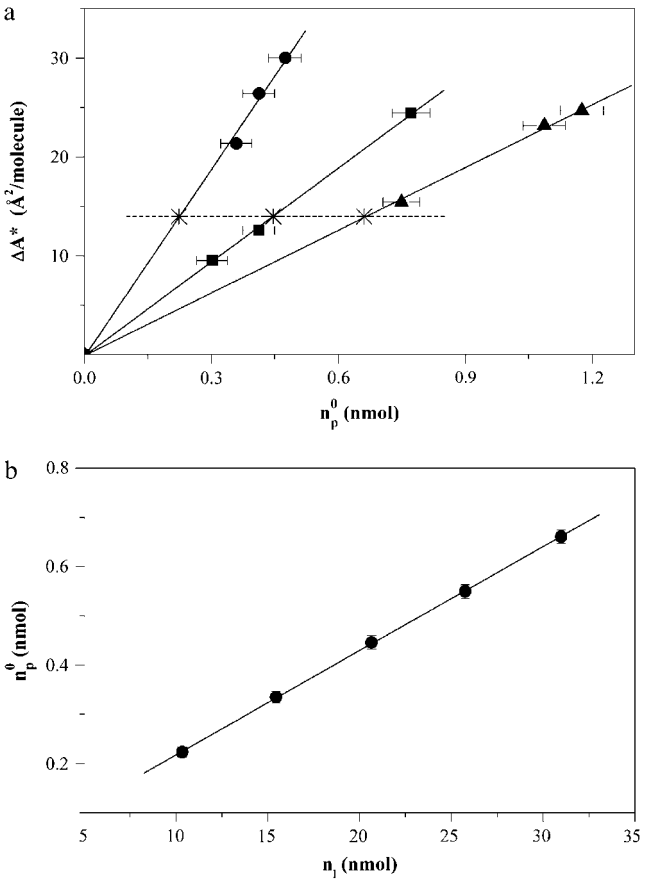

FIGURE 2 Processing of the data obtained from DMPC/MBP films. (*a*) The increase of the film area per lipid molecule, at the surface pressure of 12.5 mN/m, is plotted as a function of the total amount of added protein for films formed by different amounts of lipid, $n_l = 10.3$ nmol (●); $n_l = 20.6$ nmol (■); $n_l = 31.0$ nmol (▲). Linear equations (*continuous lines*) were fitted to the experimental data (*dots*). The larger the amount of lipid in the film, the smaller the slope of the straight line. (*b*) Mass conservation plot: n_p^o is plotted as a function of n_l at $\Delta A^* = 14$ Å^2/molecule. The set of n_p^o and n_l values was obtained from the plots reported in panel *a*. Bars indicate experimental standard errors. A linear extrapolation between experimental points has been used to increase the number of points.

The linear fit of the experimental values reported in Fig. 2 *b* provides the mixing ratio, *r*, and the amount of protein in the bulk phase, n_p^s, as the slope and the intercept of the straight line, respectively.

The data reported in Fig. 2 refer to DMPC/MBP films. Similar plots were obtained for DPPS/MBP films (not shown). For both DPPS and DMPC films, the subphase MBP concentrations resulting from the fit are compatible, within experimental error, with null bulk concentrations. This result indicates that up to surface pressures of 20 mN/m, MBP is entirely located at the interface.

In Fig. 3 *a*, the mixing ratio *r* is plotted as a function of the surface pressure for a DMPC/MBP film. The ratios were calculated for a system consisting of 21.6 nmol DMPC and 0.41 nmol MBP. As the surface pressure increases, a smooth monotonic decrease of *r* is observed. This decrease is not very marked: at the surface pressure of 2 mN/m, in the monolayer, there is 1 MBP molecule for every 42 DMPC molecules. At the surface pressure of 10 mN/m, the MBP density in the monolayer is decreased to 1 MBP molecule for every 51 DMPC molecules and remains almost constant up to a surface pressure of 20 mN/m, which is the highest surface pressure value for which this analysis is significant. The curve trend suggests that *r* should not change at higher surface pressures. Taking into account the MBP concentrations used in these experiments, <0.008 nM of MBP is pushed into the bulk phase by the surface pressure. This value is within the error of our method for measuring bulk protein concentrations. For DPPS/MBP films we have calculated *r* only at 5 mN/m and at 17 mN/m. At these surface pressures the MBP surface density is almost the same, corresponding to 1 protein molecule for every 10–11 lipid molecules, indicating a strong lipid/protein interaction less affected by the surface pressure.

The protein molecular area as a function of the surface pressure π is derived from Eq. 3. Fig. 3 *b* reports the surface pressure/area isotherm of MBP inserted into a DMPC monolayer. According to these data, as the surface pressure increases from 0 to 20 mN/m, the MBP molecular area in the lipid film is reduced, monotonically, from ~9 nm^2 to ~4 nm^2. At higher surface pressures ΔA^* vanishes, indicating that MBP is expelled from the lipid monolayer.

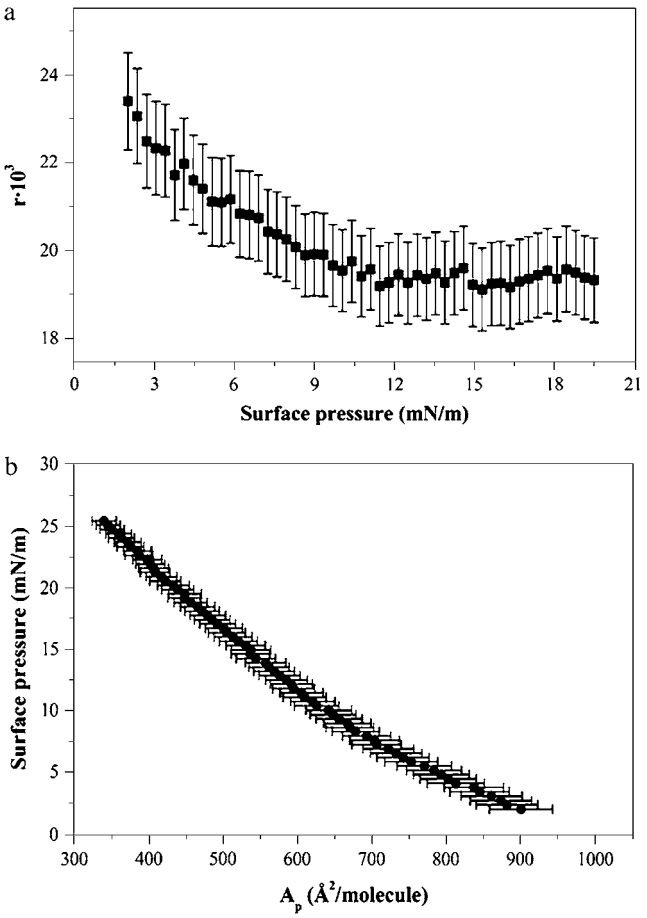

FIGURE 3 MBP in a DMPC Langmuir film. (*a*) The mixing coefficient of MBP in a DMPC monolayer is reported as a function of surface pressure. (*b*) The area per molecule of MBP in a DMPC monolayer is reported as a function of surface pressure. Bars indicate experimental standard errors.

Penetration depth determined by x-ray reflectivity measurements

To determine the penetration depth of MBP molecules into the lipid film, we performed x-ray specular reflectivity measurements on pure lipid films and protein-lipid films. The intensity of the x-ray beam scattered by a film depends on the distribution of the film electron density, and it is a function of the transfer moment (28). In the reflectivity mode the scattering angle is equal to the incidence angle; and the transfer moment, perpendicular to the film surface, is given by

$$q = \frac{4\pi \sin\theta}{\lambda}, \tag{4}$$

where θ is the incidence angle and λ is the x-ray wavelength. In reflectivity measurements, reflectivity curves are built reporting the ratio between the reflected beam intensity and the incident beam intensity as a function of the transfer moment. In our experimental apparatus the wavelength is fixed and different transfer moments correspond to different incidence angles. The mathematical expression of a reflectivity curve can be obtained modeling the film as a stack of layers of different electron densities. The model contains a few free parameters, such as the film thickness and the electron density that can be obtained by fitting the mathematical expression to the experimental data.

Fig. 4 shows the reflectivity curves of DPPS and DPPC films in the absence and in the presence of MBP at different surface pressures. The reflectivity curve of the DPPC/MBP film at a relatively low surface pressure ($\pi = 10.4$ mN/m) is very noisy, indicating a very rough film.

The lipid film was modeled as a stack of two layers of different electron densities. One layer corresponds to

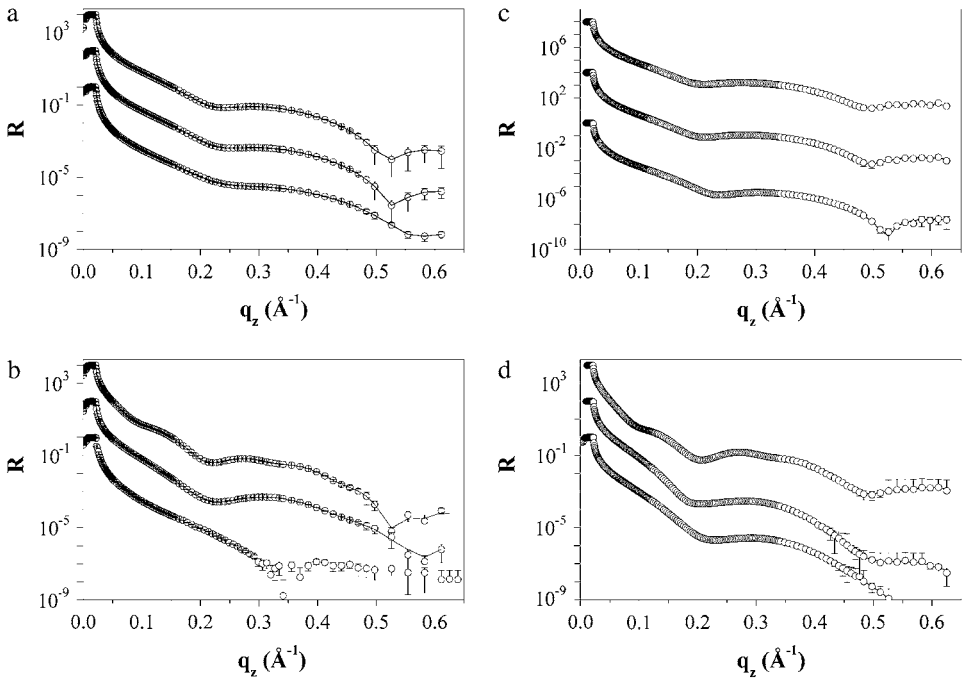

FIGURE 4 X-ray reflectivity curves of lipid and protein-lipid Langmuir films at different surface pressures. (*a*) DPPC film, surface pressures from bottom to top are 10.4 mN/m; 17.7 mN/m; and 30.8 mN/m. (*b*) DPPC/MBP film, surface pressures from bottom to top are 10.4 mN/m; 17.7 mN/m; and 30.8 mN/m. (*c*) DPPS film, surface pressures from bottom to top are 9.6 mN/m, 24.3 mN/m; and 30.6 mN/m. (*d*) DPPS/MBP film surface pressures from bottom to top are 9.6 mN/m; 24.3 mN/m; and 30.6 mN/m. Data are corrected for the background signal and normalized to the maximum value of the incident beam. For clarity, the curves obtained with the same film but at different surface pressures have been shifted with respect to each other, multiplying their values by multiples of 100. Circles represent experimental data. Continuous lines are the best fit of the Parrat formula to experimental data.

hydrophobic alkyl chains; the other corresponds to hydrophilic groups with bound water molecules. The water subphase was modeled as a third semiinfinite layer. With respect to the direction normal to the film surface (z), the electron density of these layers is a step function $\rho(z)$ consisting of three steps. This step function was smeared, modeling the electron density at the interface regions with error functions, $erf(z) = (2)/(\sqrt{\pi}) \int_0^z e^{-(t^2)/(2\sigma_i^2)} dt$. In this way, at the layer interfaces, the electron density gradients exhibit Gaussian behavior. The fit parameters are the electron densities, the thicknesses of the layers, and the σ_i of the error functions. The latter correspond to the interfacial roughnesses.

The protein-lipid film was first modeled with a two-layer model, but this model could not be fitted to the experimental data. To fit these experimental data properly, we had to add another layer between the lipid layer and the water subphase. This layer should correspond to the protein layer. Fig. 5, *a* and *c*, shows the electron densities of lipid and protein-lipid films at different surface pressures. The functions were plotted using the parameter values provided by the best fits of the reflectivity data. The derivatives of these functions are also shown (Fig. 5, *b* and *d*). According to our model, moving from left to right, maxima and minima of the derivative function correspond to the air/hydrophobic tails interface (T), the hydrophobic tails/polar heads interface (H), the polar heads/protein interface (P), and the protein/water interface (W). Comparing the electron density profiles and their derivatives at different surface pressures, one can observe that the protein is pushed out of the lipid film as the surface pressure increases. In DPPC/MBP films (Fig. 5 *b*) the distance P-W, which represents the thickness of the protein layer at the lipid/water interface, is 1.8 nm at the surface pressure of 17.7 mN/m and 4.9 nm at 30.8 mN/m. In the case of DPPS films (Fig. 5 *d*), the distance between P and W is almost stable (1.4–1.5 nm) up to a surface pressure of ~24 mN/m and then increases to ~4.8 nm at 30.6 mN/m. Therefore at high surface pressures the P-W distance is ~5 nm in both DPPS/MBP and DPPC/MBP films, whereas at surface pressure lower than 25 mN/m, it is larger for DPPC films, confirming that at low pressure MBP penetrates more in anionic lipid films.

To estimate the protein electron density profile, we subtracted the corresponding lipid contribution, obtained from lipid film measurements, from the electron density of the lipid-protein complex. Fig. 6 shows the electron density profile of MBP inserted in DPPS (Fig. 6 *a*) and DPPC films (Fig. 6 *b*). In both cases the film surface pressure before inserting the protein in the subphase was 15 mN/m. Comparing the MBP density profiles it is evident that, at surface pressures lower than 25mN/m, MBP penetrates the hydrophobic part of the anionic film, whereas it is almost entirely located at the lipid/water interface in the neutral film. These results agree with the observations of Bates et al. (14,21) and Musse et al. (22) that the electrostatic interaction plays an important role in determining the position of MBP with respect to the membrane surface.

AFM measurements

The in-plane configuration of MBP adsorbed at the water/lipid interface was studied by using AFM. The protein-lipid films were deposited on the top of five-layer LB films of DMPA; the polar part of the protein-lipid films was exposed to the AFM probe. AFM inspection was performed in water solution; the best images were obtained in tapping mode.

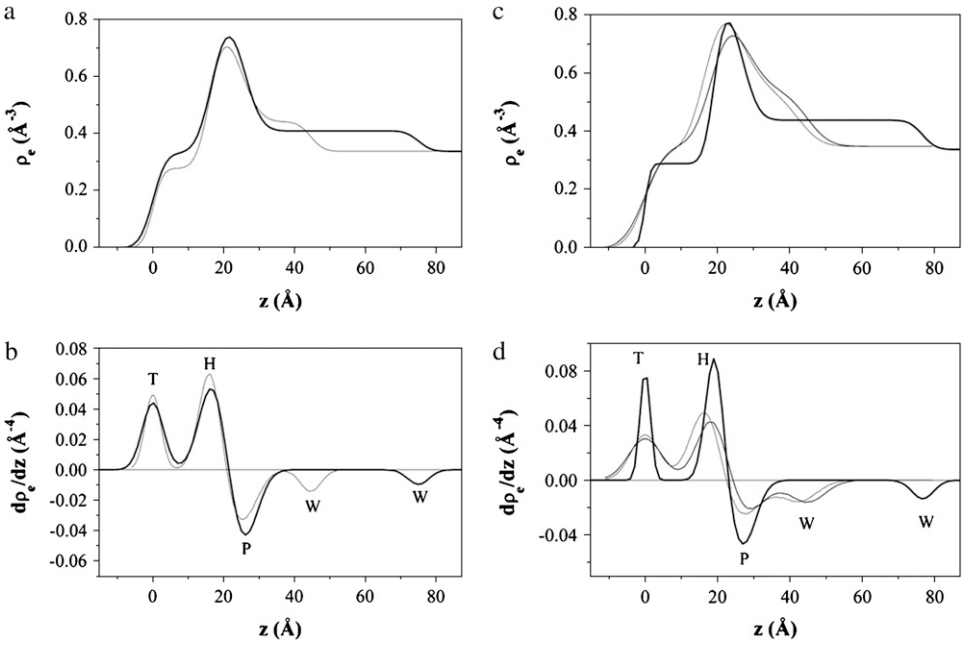

FIGURE 5 (*a*) Electron density of a DPPC/MBP film as a function of the value of the coordinate perpendicular to the film surface (z). We arbitrarily chose the origin ($z = 0$) to coincide with the air/alkyl chain interface. The thinner line is the electron density profile at $\pi = 17.7$ mN/m and the thicker line that at $\pi = 30.8$ mN/m. (*b*) Derivatives of the electron density profiles reported in panel *a*. (*c*) Electron density profiles of a DPPS/MBP film at $\pi = 9.6$ mN/m (*thin line*), $\pi = 24.3$ mN/m (*medium line*), and $\pi = 30.6$ mN/m (*thick line*). (*d*) Derivatives of the electron density profiles reported in panel *c*). In panels *b* and *d*, the extrema of the functions correspond to the interfaces between the different layers: T, air/hydrophobic tail interface; H, hydrophobic tail/polar head interface; P polar head/protein interface; and W, protein/water interface.

Fig. 7 *a* shows a DPPS monolayer (also deposited on five layers of DMPA). Fig. 7, *b* and *c*, shows the images of DPPC/MBP and DPPS/MBP films, respectively. All the images are in height mode; therefore different gray tones correspond to different levels in the surface topography. At a first qualitative inspection, the lipid and protein-lipid films are quite different. The DPPS film is characterized by flat islets typical of lipid films in an aqueous environment (16,30,31). The section profiles of these images are step functions. The analysis of the step heights indicates that the majority of the islets are 9-nm high; islets 4.5-nm high are occasionally observed. The value of 4.5 nm roughly corresponds to the thickness of a bimolecular layer; therefore the film is formed by stacks of bimolecular layers, in agreement with previous observations (16). In contrast, the surfaces of the protein-lipid films are characterized by the presence of globular, slightly elongated structures. These granules, evidently formed by MBP molecules, have different sizes and appear deposited on an almost uniform substrate. Granule size is more homogeneous in DPPS/MBP films than in DPPC/MBP films.

Since disordered surfaces are better described by the quantitative analysis of their roughness, we performed a quantitative analysis of the surface roughness of the different films. In Fig. 7 *d* we report the film roughness measured on AFM images as a function of the image scan size. The roughness of LB films, as that of many other surfaces, increases with the size of the explored area according to a scale law up to a certain cutoff length. At this length the growth stops and a roughness saturation value is reached (32). All three systems we studied are characterized by a similar behavior: the roughness increases with the scan size up to a critical length ξ (correlation length); above this value the roughness remains constant at a value σ_{sat}. Below ξ the roughness scales with the scan size, l, according to a power law of the type $\sigma \propto l^{\alpha}$. The scale exponent, the roughness saturation value, and the critical length are different for the three different films, and they are reported in Table 1. The DPPS film has the largest correlation length, the largest roughness, and the lowest scale exponent. The correlation length is quite similar in DPPS/MBP and DPPC/MBP films. The DPPC/MBP film has scale exponent and roughness larger than the DPPS/MBP film. This fact is probably due to the presence of large three-dimensional MBP clusters on the surface of the DPPC/MBP film.

The protein density is not uniform, and regions with high protein coverage coexist with regions with sparsely dispersed protein as shown in Fig. 8, where higher resolution images of different regions of a DPPS/MBP film are shown. In Fig. 8 *a* MBP granules form an almost compact layer, whereas in Fig. 8 *b* MBP granules lie scattered on the lipid surface. In both images the granules have a bean-like shape. The granules in Fig. 8 *b* are less defined than the ones in Fig. 8 *a* as the scattered granules are easily displaced by the AFM tip even when the microscope is used in tapping mode. As measured from the image cross sections, these granules are 2.3–2.5-nm high, 33-nm long, and 22-nm wide. In the AFM images the in-plane size of the granules is affected by the tip size (33). The granule height is not affected by the tip size but could be slightly modified by the deformation induced by the tip/granule interaction force; in evaluating the granule size we neglected this effect. The tip of the AFM probe can be considered spherical; therefore it does not introduce asymmetry. To evaluate the granule in-plane dimensions we modeled the granule as a hemicylinder lying on the lipid flat surface. Taking into account the measured radius of curvature of the tip, we obtained a size (h × w × l) of 2.35 ×

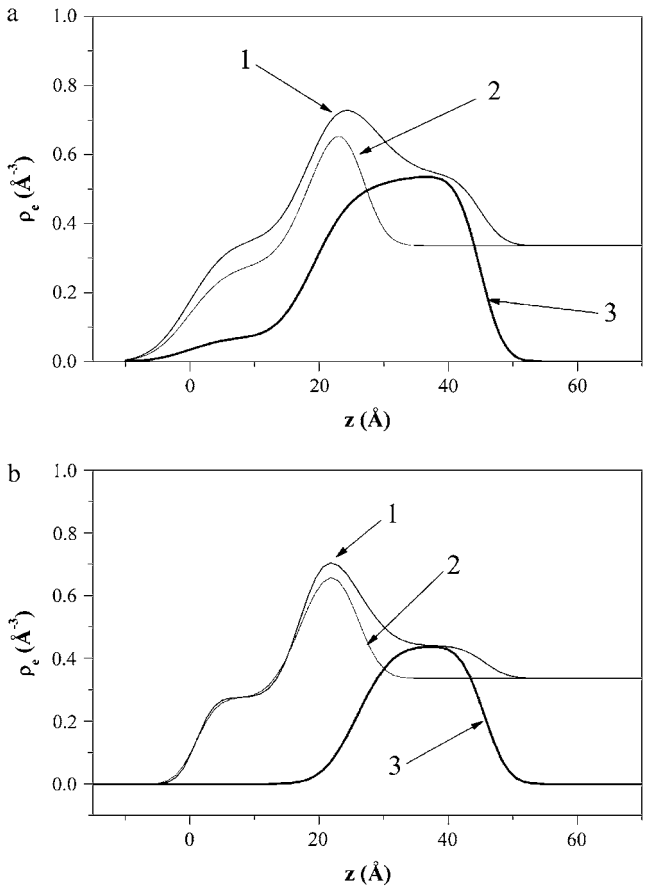

FIGURE 6 (*a*) Electron density profiles at $\pi = 24.3$ mN/m of a DPPS/MBP film (*1*), DPPS monolayer (*2*), and MBP in the DPPS film (*3*). (*b*) Electron density profile at $\pi = 17.7$ mN/m of a DPPC/MBP film (*1*), DPPC monolayer (*2*), and MBP in the DPPC film (*3*). The MBP profiles were obtained as the differences between protein-lipid film profiles (*1*) and the lipid monolayer profiles (*2*).

4.7×13.3 nm^3. Mueller et al., imaging MBP adsorbed on lipid bilayers by AFM, observed that MBP forms flat aggregates of defined height, 1.9 ± 0.2 nm on negatively and 2.7 ± 0.2 nm on positively charged lipid bilayers. These aggregates are probably monomolecular layers of MBP (34). Hu et al. observed structures 2–4-nm high formed by MBP adsorbed on mixed lipid films (35).

DISCUSSION

MBP is a soluble protein with short sequences of either neutral or hydrophobic amino acids. Even at relatively high concentration, it is not able to significantly change the surface tension of water, but it is capable of dramatically increasing the surface pressure of lipid Langmuir films at constant film area. This effect is larger for anionic lipid films and it decreases as the film surface pressure increases (6). These results indicate that MBP strongly interacts with lipids; this interaction likely induces a conformational change of the protein molecule and makes MBP act as a surfactant (6,16,19,20,36). MBP can increase the surface pressure only when it is included, at least partially, into the monomolecular lipid film. In fact screening the lipid negative charge should lead to a decrease of the surface pressure because it reduces the repulsive forces among lipid molecules. Considering the isotherms reported in Fig. 1 it is clear that MBP penetrates into the lipid films at low surface pressure both in anionic and neutral lipids. The compressibility of the protein-lipid film is larger than that of the pure lipid films; this can be caused either by the extrusion of MBP molecules from the film or by the reduction of the MBP area per molecule. Our measurements indicate that both processes occur; the second one prevails at low surface pressure. In fact, the mixing coefficient, *r*, of the DPPC/MBP film (and therefore the amount of protein at the surface; Fig. 3 *a*) is reduced only by 17% when the surface pressure is increased from 2 to 18 mN/m, whereas, in the same range of surface pressure, the MBP apparent molecular area (A_p) is reduced by ~50% (Fig. 3 *b*).

The electron density profiles of Figs. 5 and 6 show that the thickness of the protein layer at the lipid/solution interface depends on the surface pressure. It is ~1.8–1.9 nm in both DPPC and DPPS films at surface pressures lower than 25 mN/m, and it is ~5 nm at the surface pressure of 30 mN/m. At this surface pressure the electronic density profile of the lipid layer is only slightly affected by the presence of the protein; therefore MBP is almost completely confined at the interface between lipid polar heads and aqueous solution.

Cristofolini et al. (20) recently reported that MBP, when added into the subphase of a DPPG Langmuir film, drastically increases the film roughness and suppresses its reflectivity at a surface pressure as high as 35 mN/m. We observed a similar effect in the DPPC film only at relatively low surface pressure (~10 mN/m), in agreement with the fact that at low surface pressures MBP penetrates the lipid layer, destroying its order. However, according to our finding, MBP does not suppress the reflectivity of both DPPC and DPPS films at high surface pressures.

By ellipsometry, Polverini et al. measured the thickness of Langmuir films of DPPC and DPPS in the presence of MBP in the subphase at pH 6 (37). These authors observed that MBP was capable of increasing the thickness of a DPPS film in the liquid-condensed phase but not that of a DPPS film in the liquid-expanded phase. Furthermore, they observed that MBP did not affect the thickness of DPPC films both in the liquid-condensed and the liquid-expanded phase. They concluded that MBP penetrates into DPPC films in the liquid-expanded phase and it is squeezed out of the film in the liquid-condensed phase. Instead, in the case of the negatively charged DPPS, MBP penetrates into the lipid monolayer in the liquid-expanded phase, it is removed from the hydrophobic part of the film in the liquid-condensed phase, but it is kept bound to the hydrophilic part of the film by the electrostatic interaction. Furthermore, by using Fourier transform infrared spectroscopy-attenuated total reflectance measurements, they did not

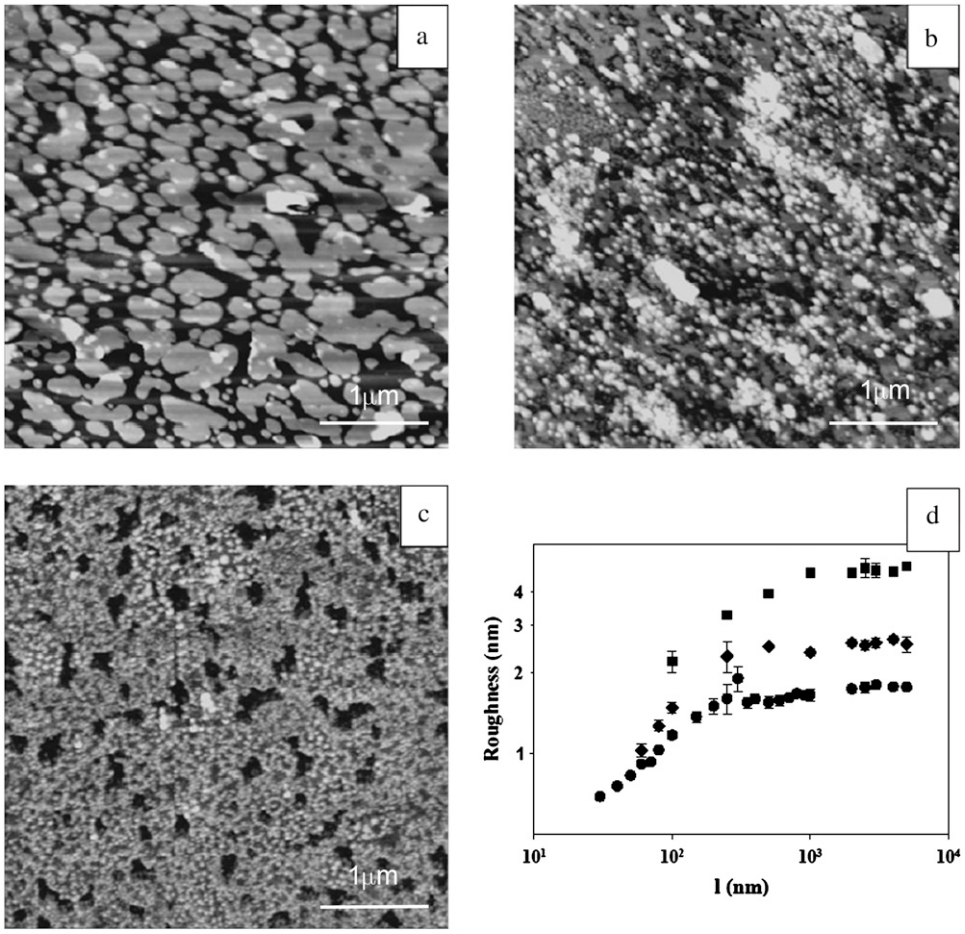

FIGURE 7 Tapping mode AFM images (height data, scan size $4 \times 4\ \mu m^2$) obtained in liquid: (*a*) DPPS LB film, *z* range 20 nm. (*b*) DPPC/MBP LB film, *z* range 10 nm. (*c*) DPPS/MBP LB film, *z* range 10 nm; and (*d*): film roughness as a function of the linear size of the scanned area. Symbols: (●) DPPS/MBP LB film; (♦) DPPC/MBP LB film; and (■) DPPS LB film. Each roughness value corresponding to a scan size value (*l*) is the average of the roughness values of different film zones having the same area (l^2). The number of the values goes from 4 for large scan sizes to >20 for small scan sizes. The error bars represent the standard errors.

observe any trace of MBP on a DPPC LB film deposited in the presence of MBP, as if MBP were only in the bulk.

Our results on DPPS/MBP films are qualitatively in good agreement with those of Polverini et al. (37), who, from ellipsometric data, evaluated the thickness of the MBP layer beneath the DPPS film to be ~3 nm at 35 mN/m. We measured a thickness of ~5 nm by x-ray reflectivity data. The different techniques and the slightly different experimental conditions can account for the difference between these two values. In the case of the interaction of MBP with uncharged lipid films, our x-ray reflectivity measurements (Figs. 4–6) and AFM inspection (Fig. 7) indicate that MBP also remains stuck to the DPPC film at high surface pressure (liquid-condensed phase). MBP forms a protein layer beneath the lipid monomolecular layer; the protein layer has about the same thickness as that formed beneath the DPPS film. MBP seems to have a stronger interaction with the negatively charged DPPS film than with the neutral DPPC film since it is inserted more deeply into the DPPS film at 24 mN/m than in the DPPC film at 17 mN/m (Fig. 6). Indirect evidence that MBP is bound with less energy to uncharged lipid films comes from AFM experiments. We observed that in the case of the DPPC/MBP film it is almost impossible to image sparse granules like those shown in Fig. 8 with sufficient resolution since granules are easily moved by the AFM tip during the scanning procedure.

MacNaughtan and co-workers found that in cerebroside LB films deposited at surface pressures larger than 30 mN/m, MBP forms a layer ~3-nm thick between the lipid polar heads (18). A value of 1.0 nm is reported by Haas and co-workers for DLPA LB film deposited at a similar surface pressure (19). These values are smaller than the values for MBP layers beneath DPPC and DPPS films at 30 mN/m, possibly due to rearrangement of the protein induced by the presence of another lipid layer.

Mueller et al. (34) suggested that MBP is adsorbed on a acidic lipid film according to an adsorption-diffusion mechanism. Solvated MBP molecules adsorb to the lipid bilayer

TABLE 1 Parameters derived from the analysis of the roughness of AFM images of DPPS/MBP, DPPC/MBP, and DPPS films (Fig. 7 *d*); α is the scaling exponent, σ_{sat} is the saturation roughness, and ξ is the critical length

Film	α	σ_{sat} (nm)	ξ (nm)
DPPS/MBP	0.45 ± 0.02	1.71 ± 0.05	~200
DPPC/MBP	0.710 ± 0.013	2.7 ± 0.2	~200
DPPS	0.35 ± 0.05	4.8 ± 0.2	~800

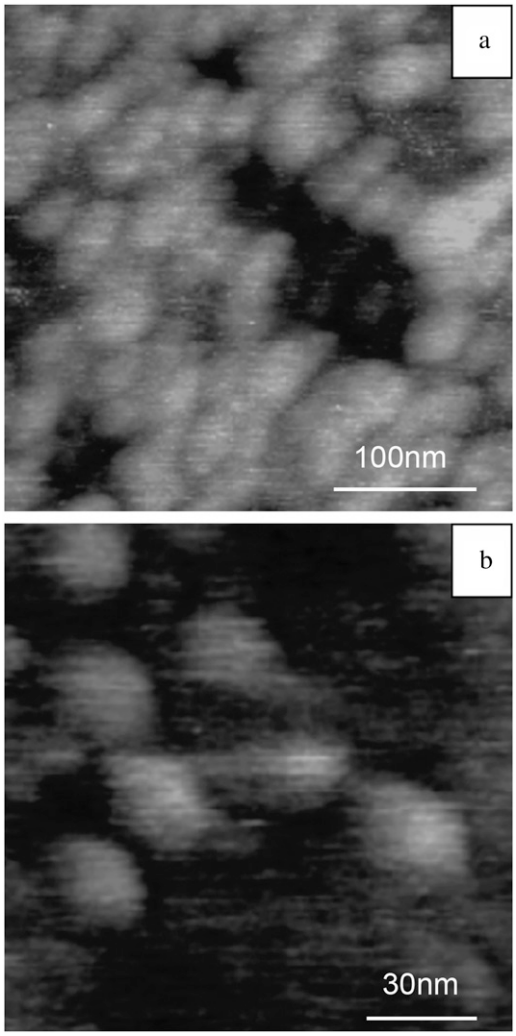

FIGURE 8 AFM height images of two different regions of a DPPS/MBP L-B film: (*a*) an almost compact layer of MBP clusters, scan size 360 × 360 nm^2, *z* range 10 nm; and (*b*) scattered MBP clusters, scan size 140 × 140 nm^2, *z* range 8 nm. The cluster size in the scan plane is affected by the tip size (see text).

and refold. The adsorbed molecules can diffuse on the bilayer. An attractive interaction between the adsorbed molecules leads to the formation of MBP monolayers on the lipid film. A similar mechanism is also compatible with the results reported by Shanshiashvili et al. (38), who studied the adhesion of MBP isomers to phosphatidylcholine/phosphatidylserine model membranes using waveguide lightmode spectrometry. These authors observed that the isomer C1, which has the largest positive charge, specifically undergoes compaction upon adsorption from the most concentrated solution. The growth process of the protein layer could be revealed by the roughness scaling law (39). The film roughness and scaling exponents reported in Table 1 cannot be associated with this growth process nor with the growth process of cadmium arachidate LB films inspected in dry conditions (32), but they suggest a few important facts: MBP is able to induce lateral compaction of lipid surfaces. Multilayer lipid films undergo surface reconstruction, forming irregular bilayer stacks when kept in aqueous environment (16,30,31). MBP reduces dramatically the film roughness (Fig. 7 *d*) and changes the structure of the film surface as indicated by the different values of scaling exponents and critical lengths. This result is in agreement with previous AFM observations indicating that the adsorption of MBP on lipid layers has the effect of healing defects and filling holes (34,35). We can envisage that MBP stabilizes the surface structure of the lipid film, hindering the surface reconstruction.

We also observed sparse granules which might be single molecules. These granules are not dissimilar from the granules observed by Bates et al. on the periphery of lamellar structures (14). Beniac et al. (13) reported that the MBP molecule on the lipid polar surface has a semitoroidal or c shape with a inner radius of 3 nm, an external radius of 5.5 nm, and a thickness of 4.7 nm. The standard AFM tip that we use is too big to penetrate and image the inner hollow site of this toroid, and its image would result in a bean-shaped granule with dimensions similar to those we have estimated. The granule size in Fig. 8 is also compatible with a pair of molecules interpenetrated in the way suggested by Shanshiashvili and co-workers (38). We measure a granule thickness of 2.35 nm, which is smaller than the thickness evaluated in Riccio et al. (10). A partial penetration in the lipid layer and molecule deformation induced by the AFM probe could be responsible for this smaller value. On the other hand, imaging of MBP on lipid films in different conditions, as well as information coming from spectroscopic techniques, suggests that MBP is a very flexible molecule which can form different structures in association with lipids (14–16,34–36). Also in our case we cannot rule out that the observed structures are lipid/protein aggregates. The lipid membrane composition as well as its physical state (temperature, fluidity, charge) are likely to affect the MBP molecular conformation. Furthermore, different isomers can either assume different conformations or interact differently with the lipid film (9,21,22,38).

CONCLUSIONS

Notwithstanding that MBP is a soluble protein, in the presence of a phospholipid film it is located predominately at the water solution interface. The affinity of MBP for the lipid/water interface is not due only to electrostatic interactions since it also occurs with neutral lipids. The MBP/lipid film interaction depends on the film surface pressure. At low surface pressure MBP penetrates both anionic and neutral lipid films, increasing the lipid area per molecule. This increase is reduced by increasing the surface pressure. Two processes contribute to this decrease: a few protein molecules are gradually expelled from the film and the area per molecule of the protein in the film is gradually reduced. Up to a surface pressure of ~20 mN/m the second process predominates. At

surface pressures as high as 30 mN/m, MBP molecules are almost completely located at the lipid/water interface both in anionic and neutral lipid films. AFM images show that MBP reduces the roughness and correlation length of LB films deposited at 35 mN/m, forming a granular layer of clusters of molecules. The density of this MBP layer is not uniform, and regions exist in which scattered granules of bean-like shape are observed. The size of these granules is compatible with that of either a MBP single molecule or a pair of interpenetrated molecules; however, we cannot rule out that they are lipid-protein complexes. These sparse molecules do not seem tightly bound to the lipid surface since they are dragged by the AFM probe even when it is used in tapping mode.

The choice of very simple lipid systems allowed us to obtain experimental evidence that the interaction of MBP with lipid membranes is modulated by lipid charge and surface tension, which determine the molecular conformation of MBP. We believe that the methods reported in this article will be able to reveal differences in the interactions of the different isomers of MBP with lipid membranes, relating their biophysical properties to their physiological role and possibly to their role in demyelination in multiple sclerosis.

We thank Nadia Marano for carefully reading the manuscript and for her invaluable suggestions.

This work was carried out within the framework and the activities of the MARIE Network of the European Science Foundation on Myelin Structure and Its Role in Autoimmunity. We acknowledge the support by the University of Genoa through ''Progetti di Ateneo''.

REFERENCES

1. Inouye, H., and D. A. Kirschner. 1984. Effects of $ZnCl_2$ on membrane interactions in myelin of normal and shiverer mice. *Biochim. Biophys. Acta.* 776:197–208.
2. Inouye, H., J. Karthigasan, and D. A. Kirschner. 1989. Membrane structure in isolated and intact myelins. *Biophys. J.* 56:129–137.
3. Luzzati, V., and L. Mateu. 1990. Order-disorder phenomena in myelinated nerve sheaths. *J. Mol. Biol.* 215:373–384.
4. Lodish, H., D. Baltimore, A. Berk, S. L. Zipursky, P. Matsudaira, and J. Darnell. 1995. Molecular Cell Biology, 3rd ed. Scientific American Books. W. H. Freeman and Company, New York. 941–942.
5. King, R. H. M., and P. K. Thomas. 1984. The occurrence and significance of myelin with unusually large periodicity. *Acta Neuropathol. (Berl.).* 63:319–329.
6. Demel, R. A., Y. London, W. S. M. Geurts van Kessel, F. G. A. Vossemberg, and L. L. M. van Deenen. 1973. The specific interaction of myelin basic protein with lipids at the air-water interface. *Biochim. Biophys. Acta.* 311:507–519.
7. Smith, R. 1992. The basic-protein of CNS myelin. Its structure and ligand-binding. *J. Neurochem.* 59:1589–1608.
8. Nabet, A., J. M. Boggs, and M. Pézolet. 1994. Study by infrared spectroscopy of the interaction of bovine myelin basic protein with phosphatidic acid. *Biochemistry.* 33:14792–14799.
9. Bates, I. R., J. M. Boggs, J. B. Feix, and G. Harauz. 2003. Membrane-anchoring and charge effects in the interaction of myelin basic protein with lipid bilayers studied by site-directed spin labeling. *J. Biol. Chem.* 278:29041–29047.
10. Riccio, P., J. P. Rosenbusch, and E. Quagliariello. 1984. A new procedure to isolate brain myelin basic protein in a lipid-bound form. *FEBS Lett.* 177:236–240.
11. Polverini, E., A. Fasano, F. Zito, P. Riccio, and P. Cavatorta. 1999. Conformation of bovine myelin basic protein purified with bound lipids. *Eur. Biophys. J.* 28:351–355.
12. Haas, H., C. L. P. Oliveira, I. L. Torriani, E. Polverini, A. Fasano, G. Carlone, P. Cavatorta, and P. Riccio. 2004. Small angle x-ray scattering from lipid-bound myelin basic protein in solution. *Biophys. J.* 86:455–460.
13. Beniac, D. R., M. D. Luckevich, G. J. Czarnota, T. A. Tompkins, R. A. Ridsdale, F. P. Ottensmeyer, M. A. Moscarello, and G. Harauz. 1997. Three-dimensional structure of myelin basic protein. I. Reconstruction via angular reconstitution of randomly oriented single particles. *J. Biol. Chem.* 272:4261–4268.
14. Bates, I. R., P. Matharu, N. Ishiyama, D. Rochon, D. D. Wood, E. Polverini, M. A. Moscarello, N. J. Viner, and G. Harauz. 2000. Characterization of a recombinant murine 18.5-kDa myelin basic protein. *Protein Expr. Purif.* 20:285–299.
15. Ishiyama, N., I. R. Bates, C. M. Hill, D. D. Wood, P. Matharu, N. J. Viner, A. Moscarello, and G. Harauz. 2001. The effects of deimination of myelin basic protein on structures formed by its interaction with phosphoinositide-containing lipid monolayers. *J. Struct. Biol.* 136: 30–45.
16. Lanteri, N., R. Rolandi, P. Cavatorta, E. Polverini, P. Riccio, and A. Gliozzi. 2000. Myelin basic protein-lipid complex: an atomic force microscopy study. *Colloids Surf. A. Physicochem. Eng. Asp.* 175:3–9.
17. Murthy, N. S., D. D. Wood, and M. A. Moscarello. 1984. X-ray scattering studies of a model complex of lipid and basic protein of myelin. *Biochim. Biophys. Acta.* 769:493–498.
18. MacNaughtan, W., K. A. Snook, E. Caspi, and N. P. Franks. 1985. An x-ray diffraction analysis of oriented lipid multilayers containing basic proteins. *Biochim. Biophys. Acta.* 818:132–148.
19. Haas, H., M. Torrielli, R. Steitz, P. Cavatorta, R. Sorbi, A. Fasano, P. Riccio, and A. Gliozzi. 1998. Myelin model membranes on solid substrates. *Thin Solid Films.* 327–329:627–631.
20. Cristofolini, L., M. P. Fontana, F. Serra, A. Fasano, P. Riccio, and O. Konovalov. 2005. Microstructural analysis of the effect of incorporation of myelin basic protein in phospholipid layers. *Eur. Biophys. J.* 34:1041–1048.
21. Bates, I. R., J. B. Feix, J. M. Boggs, and G. Harauz. 2004. An immunodominant epitope of myelin basic protein is an amphipathic α-helix. *J. Biol. Chem.* 279:5757–5764.
22. Musse, A. A., J. M. Boggs, and G. Harauz. 2006. Deimination of membrane-bound myelin basic protein in multiple sclerosis exposes an immunodominant epitope. *Proc. Natl. Acad. Sci. USA.* 103:4422–4427.
23. Schwarz, G. 2000. A universal thermodynamic approach to analyze biomolecular binding experiments. *Biophys. Chem.* 86:119–129.
24. Schwarz, G., and S. E. Taylor. 1999. Polymorphism and interactions of a viral fusion peptide in a compressed lipid monolayer. *Biophys. J.* 76:3167–3175.
25. Deibler, G. E., R. E. Martenson, and M. W. Kies. 1972. Large scale preparation of myelin basic protein from central nervous tissue of several mammalian species. *Prep. Biochem.* 2:139–165.
26. Liebes, L. F., R. Zand, and W. D. Phillips. 1975. Solution behavior, circular dichroism and 220 Mz PMR studies of the bovine myelin basic protein. *Biochim. Biophys. Acta.* 405:27–39.
27. D'Acapito, F., I. Emelianov, A. Relini, P. Cavatorta, A. Gliozzi, V. Minicozzi, S. Morante, P. L. Solari, and R. Rolandi. 2002. Total external reflection x-ray absorption spectroscopy reveals zinc coordination shell in phospholipid Langmuir-Blodgett films. *Langmuir.* 18: 5277–5282.
28. Als-Nielsen, J. 1985. The liquid vapour interface. *Z. Phys. B.* 61: 411–414.
29. Reference deleted in proof.
30. Cappella, B., P. Baschieri, M. Ruffa, C. Ascoli, A. Relini, and R. Rolandi. 1999. Structure and nanomechanical properties of solvent cast stearic acid films in liquid: an AFM study. *Langmuir.* 15:2152–2157.

31. Schwartz, D. K., J. Garnaes, R. Viswanathan, and J. A. N. Zasadzinski. 1992. Surface order and stability of Langmuir-Blodgett-films. *Science*. 257:508–511.

32. Basu, J. K., S. Hazra, and M. K. Sanya. 1999. Growth mechanism of Langmuir-Blodgett films. *Phys. Rev. Lett.* 82:4675–4678.

33. Keller, D. 1991. Reconstruction of STM and AFM images distorted by finite-size tips. *Surf. Sci.* 253:353–364.

34. Mueller, H., H.-J. Butt, and E. Bamberg. 2000. Adsorption of membrane-associated proteins to lipid bilayers studied with an atomic force microscope: myelin basic protein and cytochrome *c*. *J. Phys. Chem. B*. 104:4552–4559.

35. Hu, Y., I. Doudevski, D. Wood, M. Moscarello, C. Husted, C. Genain, J. A. Zasadzinski, and J. Israelachvili. 2004. Synergistic interactions of lipids and myelin basic protein. *Proc. Natl. Acad. Sci. USA*. 101:13466–13471.

36. Khattari, Z., Y. Rushel, H. Z. Wen, A. Fischer, and T. M. Fischer. 2005. Compactification of a myelin mimetic Langmuir monolayer upon adsorption and unfolding of myelin basic protein. *J. Phys. Chem. B*. 109:3402–3407.

37. Polverini, E., S. Arisi, P. Cavatorta, T. Berzina, L. Cristofolini, A. Fasano, P. Riccio, and M. Fontana. 2003. Interaction of myelin basic protein with phospholipid monolayers: mechanism of protein penetration. *Langmuir*. 19:872–877.

38. Shanshiashvili, L. V., N. Ch. Suknidze, G. G. Machaidze, D. G. Mikeladze, and J. J. Ramsden. 2003. Adhesion and clustering of charge isomers of myelin basic protein at model myelin membranes. *Arch. Biochem. Biophys*. 419:170–177.

39. Barabási, A.-L., and H. E. Stanley. 1995. Fractal Concepts in Surface Growth. Cambridge University Press, Cambridge.